Gaussian derivative wavelet propagation in a single scattering bubbly water beyond resonant frequency

Yves Le Gonidec

Gaussian derivative wavelet propagation in a single scattering bubbly water beyond resonant frequency

Yves Le Gonidec

1 February 2023

Univ. Rennes, CNRS, Géosciences Rennes, UMR 6118, 35000 Rennes, France
Yves.LeGonidec@univ-rennes1.fr

Abstract

Acoustic pulses transmitted across air bubbles in water are usually analyzed in the ν frequency domain to determine the attenuation coefficient and phase velocity for comparison with scattering and effective models. In the present work, acoustic experiments performed beyond the bubble resonant frequency in the single scattering regime highlight an amplitude decrease and a significant shape variability of the waveform with the propagation distance x, but also a nearly constant normalized amplitude spectrum. The amplitude spectrum can be characterized by a fractional derivative order $\gamma_x = \kappa_\gamma x$, with κ_γ a constant defined by a numerical optimization method, and a time dilation factor δ_x which effects compensate. The phase spectrum is shifted by $\frac{\pi}{2}\gamma_x$ and explains the experimental waveform changes. The phase velocity can be approximated to $\tilde{v}_0/(1-\kappa_\gamma \tilde{v}_0/4\nu)$, where $\tilde{v}_0$ is similar to the sound speed in water. It is also shown that the waveform shape, quantified by γ_x, is correlated to the waveform amplitude. The results highlight potential interests in underwater communication.

1 Introduction

In underwater acoustics, a wave may be drastically affected by the presence of bubbles which act as strong scatterers [1]. A single bubble is characterized by a low-frequency resonance ν_r, typically 3 kHz for a 1 mm radius air bubble in water as firstly quantified in the 1930s by Minnaert and intensively considered since then [2, 7]. For a bubble cloud, the bubbly water is characterized by an effective complex wavenumber which real and imaginary parts are related to the phase velocity $v(\nu)$ and attenuation coefficient $\alpha(\nu)$, respectively. Many physical phenomena and bubble properties can be considered when modeling v and α, including multiple scattering and bubble-bubble interactions [4, 8, 15, 26, 29], encapsulating shell and bubble shape [14, 18, 23, 24] and polydispersity [11].

Because of this complexity, various experimental works have been performed since many years to measure v and α and compare the results with effective models in the frequency domain [6, 13, 17, 27, 32].

Some publications illustrate the acoustic signals in the time domain [9, 10, 22, 28]. For instance, [22] show a 50 kHz acoustic pulse transmitted through a bubbly gel composed of 0.15% volume fraction of 81 μm radius bubbles: the shape of the transmitted signal is more complex than the pulse shape. A quantitative relationship between this complexity and the dispersive character of the bubbly gel is not obvious since the measurement had been performed near resonance where attenuation and phase velocity change significantly with the frequency [12]. For a weak attenuation that linearly increases with the frequency [16], waveform changes can be attributed to fractional integration effects [19]. This may be not the case in the bubbly medium at frequencies far beyond the bubble resonant frequency where the attenuation is weak but follows a decreasing trend with the frequency. In the present work, a 310 kHz acoustic pulse propagates in a bubbly water composed of roughly 0.2% volume fraction of 1.6 mm radius air bubbles ($\nu_r \simeq$2 kHz): the study focuses on analytical descriptions of phenomenological effects that affect the acoustic waveform.

The laboratory acoustic experiments are described in Section 2 to introduce qualitative changes of the acoustic waveforms associated to a propagation distance $x \leq$740 mm inside the bubbly water. In Section 3, the attenuation of the waveform amplitude as a function of x is quantified in the time domain, and α and v are measured in the frequency domain to be compared with effective models. Section 4 deals with analytical developments based on Gaussian derivative properties of a model source wavelet: fractional derivation and dilation parameters are introduced from an approximation of α at high frequencies and used to approximate v accordingly to model the acoustic waveform across the dispersive medium. The analysis is extended to the experimental waveforms in Section 5 where the correlation between the shape and amplitude of the waveforms is highlighted in agreement with the modeling. Conclusion and perspective for future studies are presented in Section 6.

2 Description of the acoustic experiments

Two series of experiments have been performed in an acoustic tank filled with 5 m^3 of tap water: one in pure water (non-dispersive homogeneous medium) and one in bubbly water (dispersive biphasic medium).

2.1 Acoustic waveforms measured in pure water

A piezo-electric transducer, with a central frequency of 500 kHz and an active face that acts as a circular plane piston of radius R=1.5 cm, is used to emit an acoustic pulse into the so-called reference pure water. A similar transducer is placed in front of the emitter to record the transmitted acoustic signal. The waveform $W_0(t)$ recorded at the distance x_0=365 mm represents the reference signal in the following (Fig. 1a1). As a first approximation, the waveform is composed of 5 extrema: it is symmetric relative to the main peak which defines

the center of the waveform and is arbitrary set to 1 (normalized amplitude at x_0). The signal is a superposition of plane waves with harmonic time dependence according to the Fourier transform, *i.e.*

$$\hat{W_0}(\nu) = \frac{1}{2\pi} \int_{-\infty}^{\infty} W_0(t) e^{-i2\pi\nu t} dt, \tag{1}$$

which modulus is maximum at the peak frequency $\nu_{p_0} \simeq$310 kHz (Fig. 1a4). Note that the measurements are performed in the far field condition $x_0 > R^2/4\lambda$, where λ is the acoustic wavelength in water. The measurements are performed for successive positions x of the receiver (Fig. 1a2). The position is defined from the time-of-flight of the transmitted signal in water (sound speed v_0=1473 m.s^{-1}) and ranges between x_0 and x_0+840 mm. The dataset consists in 221 acoustic waveforms $W_x(t)$ acquired with a sampling rate of 10 MHz. By both correcting the waveform amplitude from the spherical divergence of the acoustic beam and time shifting the amplitude peak at t=0, the waveforms measured in pure water are all similar to $W_0(t)$ (Figs. 1a2): in particular, the symmetry of the waveform and the amplitude spectrum do not depend on the distance x as expected for a non dispersive medium (Figs. 1a3 and 1a4).

2.2 Acoustic waveforms measured in bubbly water

The dataset of the second experiment has been acquired when air bubbles are being released in the pure water to create a dispersive biphasic medium. Bubbles are released by the use of an artificial generator composed of 8 parallel identical pierced tubes, 10 cm apart, filled with air under a pressure of 1.4 bars (Fig. 2a). Each tube, 8 mm in diameter, has been pierced of 26 holes, 2 cm apart, to create a bubble cloud in the water. The distance between the acoustic emitter and the first tube is 100 mm, *i.e.* the recorded waveform at the initial position x_0 is $B_0(t) = W_0(t)$ (Fig. 1b1). The trajectory of the bubbles rising up to the surface is not straight and fluctuates in the vicinity of each tube: as a first approximation, the instantaneous bubble distribution is homogeneous. Bubbles are ellipsoidal (Fig. 2a), with half minor axes between 1 and 3 mm and an eccentricity about 1.5 (Fig. 2b). Measurements are not accurate but not critical for the present study and a bubble is approximated to a fluid sphere which radius is half the minor axis, in average normal to the acoustic beam. A log-normal distribution highlights a median value r_0=1.6 mm and a polydispersity ϵ=20% (Fig. 2c). The gas volume fraction of the biphasic medium is estimated from $\frac{4}{3}\pi r_0^3 N_b N_t/V$ where $N_b \simeq$11 is the number of bubbles in one picture, N_t=8 is the number of tubes, and $V \simeq$1.5 l is the volume associated to the picture surface multiplied by the length 740 mm of bubbly water. As a rough estimate, the bubbly liquid is characterized by 0.15% volume fraction of 1.6 mm radius air bubbles with a 20% polydispersity in pure water where the sound speed is about 1473 m.s^{-1}.

The mean acoustic field is measured by averaging 200 signals that propagate through different realizations of the dynamic bubbly water. The dataset of the second experiment consists in 221 average acoustic waveforms $B_x(t)$ measured for different propagation distances x and both corrected in amplitude from the spherical spreading and time-shifted to

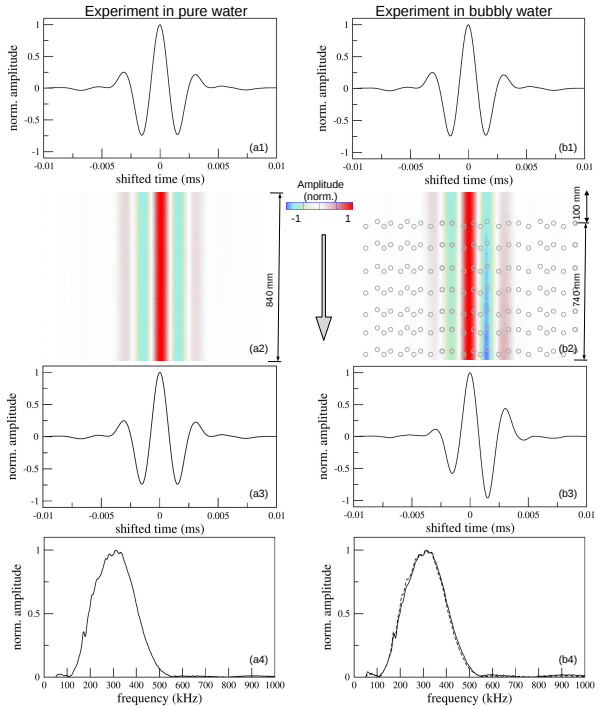

Figure 1: Experimental waveforms measured (left) in pure water and (right) in bubbly water: (a1 and b1) reference source signals and (a2 and b2) transmitted waveforms measured at 211 successive positions x. The waveforms are displayed with a normalized amplitude and an arbitrary time reference. (a3 and b3) Last transmitted waveforms and (a4 and b4) associated amplitude spectra (solid curve). Note that the amplitude spectrum measured in the bubbly water is similar to the one of the reference signal (b4, dashed curve).

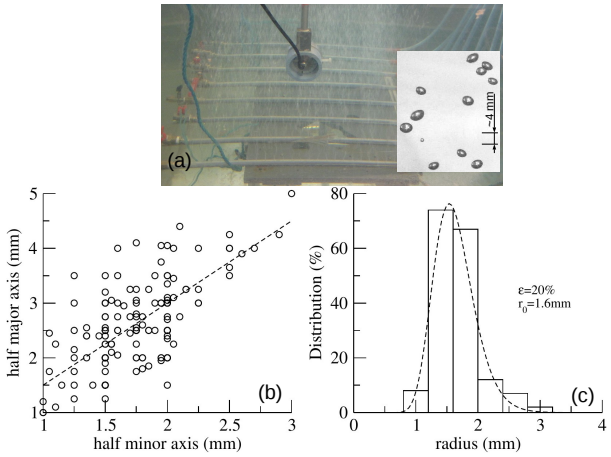

Figure 2: (a) Photographs of the 8 bubble clouds and few bubbles (inset picture). (b) Major and minor axes of elliptical bubbles (circles). (c) Experimental and log-normal (dashed curve) size distributions.

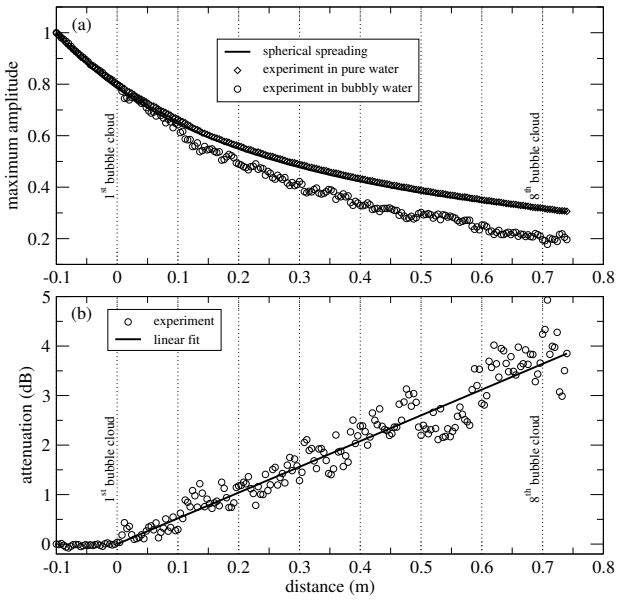

Figure 3: (a) Decreasing trend of the waveform amplitude in pure water (diamonds), in accordance with the spherical spreading of the acoustic wave (solid curve), and in bubbly water (circles) as a function of the distance x. (b) Attenuation in dB induced by the bubbles as a function of x (circles) and linear fit (solid line).

align the amplitude peak at t=0 (Fig. 1b2). As a key observation, the waveform $B_x(t)$ is not constant with x: in particular, the symmetry is progressively lost when the propagation distance inside the bubbly water increases from 0 to 740 mm (Figs. 1b2 and 1b3) but the amplitude spectrum is not modified (Fig. 1b4).

This highlights qualitative results on the continuous modification of the average acoustic waveform when the acoustic wave propagates inside the bubbly water. To better understand the interaction between the acoustic wave and the bubbles, a quantitative analysis is described in the following, based on effective medium models to characterize the bubbly water in terms of attenuation and phase velocity.

3 Experimental attenuation and phase velocity

3.1 Analysis in the time domain

In pure water, the maximum amplitude $M_W(x)$ of the waveform $W_x(t)$ decreases as the spherical spreading $1/x$ (Fig. 3a, diamonds and solid curve, respectively): intrinsic attenuation of the acoustic wave propagating in the water can be neglected. In bubbly water, the decrease of the maximum amplitude $M_B(x)$ of the waveforms $B_x(t)$ (Fig. 3a, circles) is stronger than the spherical spreading when $x > 0$ which corresponds to the location of the first bubble cloud.

The attenuation of the acoustic wave can be quantified in dB according to $-20\log_{10}\left(M_B(x)/M_W(x)\right)$

(Fig. 3b, circles). Despite the average measurements performed on many realizations of bubble clouds, the results are scattered: as a first approximation, the attenuation linearly increases with x (Fig. 3b, solid line), about 5.2 dB.m^{-1} for ν_{p_0}=310 kHz. Better estimates of the bubbly water properties, *i.e.* both attenuation coefficient and phase velocity as functions of the acoustic frequency, are assessed in the frequency domain.

3.2 Analysis in the frequency domain

In pure water, an acoustic wave of angular frequency $\omega = 2\pi\nu$ propagates at a constant speed v_0 with a real wavenumber $k_0 = \omega/v_0$. In the Fourier domain, the acoustic plane-wave measured at x is given by:

$$\hat{W}_x(\nu) = \hat{W}_0(\nu)e^{i(2\pi\nu t - k_0 x)} = \hat{W}_0(\nu)e^{i2\pi\nu\left(t-\frac{x}{v_0}\right)}. \tag{2}$$

In bubbly water, the acoustic wave propagates with a frequency dependent complex wavenumber $k(\nu)$ which real and imagery parts are defined by an attenuation coefficient $\alpha(\nu)$ and a phase velocity $v(\nu)$, respectively, according to:

$$k(\nu) = \frac{2\pi\nu}{v(\nu)} - i\alpha(\nu) \tag{3}$$

and the acoustic plane-wave measured after a propagation distance x inside the bubbly water is thus given by:

$$\hat{B}_x(\nu) = \hat{B}_0(\nu)e^{i(2\pi\nu t - kx)} \tag{4a}$$

$$= \hat{B}_0(\nu)e^{-\alpha x}e^{i2\pi\nu\left(t-\frac{x}{v}\right)} \tag{4b}$$

$$= \hat{W}_x(\nu)e^{-\alpha x}e^{i2\pi\nu\left(\frac{x}{v_0}-\frac{x}{v}\right)}. \tag{4c}$$

The attenuation coefficient is related to the ratio of the moduli $|\hat{B}_x(\nu)|$ and $|\hat{W}_x(\nu)|$ and the phase velocity to the phase shift $\Delta\Phi = arg(\hat{B}_x(\nu)) - arg(\hat{W}_x(\nu))$ which gives:

$$\alpha(\nu) = -\frac{1}{x}\ln\frac{|\hat{B}_x(\nu)|}{|\hat{W}_x(\nu)|} \tag{5a}$$

$$v(\nu) = \frac{xv_0 2\pi\nu}{x2\pi\nu - v_0\Delta\Phi}. \tag{5b}$$

For frequencies close to $\nu_{p_0} \gg \nu_r$ (Fig. 4, dotted curve), the experiments highlight very weak dependencies of both α and v with ν (Fig. 4, circles).

3.3 Effective medium modeling of the bubbly water

The bubbly water is a biphasic system composed of air bubbles in a fluid matrix and is characterized by a theoretical effective complex wavenumber $k(\nu)$ related to the physical properties of the medium by the use of an effective medium modeling.

The model developed by [12] is widely used in the 'Independent Scattering Approximation' for dilute systems characterized by both a mean distance d between the bubbles much larger than the acoustic wavelength λ and isotropic scatterers with a radius $r < \lambda$. In this case, the polydisperse bubbly water is modeled by the effective complex wavenumber k_F:

$$k_F^2 = k_0^2 + 4\pi \int N(r)H(r)dr. \tag{6}$$

The term $N(r)$ is the log-normal distribution of the bubble size and $H(r)$ the far-field isotropic scattering amplitude of a single bubble of radius r defined by [5, 33]

$$H(r) = \frac{r}{\frac{\nu_r^2}{\nu^2} - 1 + i\delta} \tag{7}$$

where $\delta = \delta_r + \delta_t + \delta_v$ is the damping factor of a single bubble, comprising the acoustic radiation (δ_r), the thermal effects (δ_t) and the viscosity (δ_v) [25]. The resonant frequency $\nu_r = \frac{1}{2\pi}\sqrt{\frac{3\gamma P_0}{r^2\rho_0}}$ is the so-called Minnaert frequency of a bubble of radius r, with $\gamma = 1.4$ the ratio of air heat capacities, P_0=0.1 MPa the air static pressure and ρ_0=1000 kg.m^{-3} the water mass density. Note that for the radius r_0=1.6 mm, a single bubble resonates at $\nu_r \simeq$2 kHz, which is much lower than the peak frequency ν_{p_0}=310 kHz of the reference source signal $B_0(t)$.

In the model developed by [20], the isotropic scattering amplitude H is replaced by the forward scattering amplitude H_0 of a fluid sphere in order to take anisotropic scatterers into account when $\lambda < r$. The wavenumber is given by

$$k_L^2 = k_0^2 + 4\pi \int N(r)H_0(r)dr \tag{8}$$

where $H_0(r)$ is a complex function that depends on the Legendre polynomials and the Neumann and Bessel functions [3].

The model developed by [31] takes into account multiple scattering interactions between the acoustic wave and the biphasic system composed of anisotropic scatterers. When the condition $d >> \lambda$ required for the two previous models is not satisfied, the effective wavenumber of the bubbly water can be modeled by:

$$k_{WT}^2 = k_L^2 + \frac{1}{4k_0^2}(4\pi)^2 \int N(r)^2 \left(H_0^2(r) - H_\pi^2(r)\right) \tag{9}$$

where $H_0(r)$ and $H_\pi(r)$ defined by [3] stand for the forward and backward scattering functions of a single bubble, respectively.

The complex wavenumbers are computed by considering the physical parameters of the experiment, including the median bubble radius r_0=1.6 mm and the polydispersity ϵ=20%: only the volume fraction initially estimated about 0.15% has been increased to ϕ=0.2% to better fit the model and experimental results. The modeled wavenumber based on k_F predicts an attenuation that strongly depends on the frequency and underestimates the

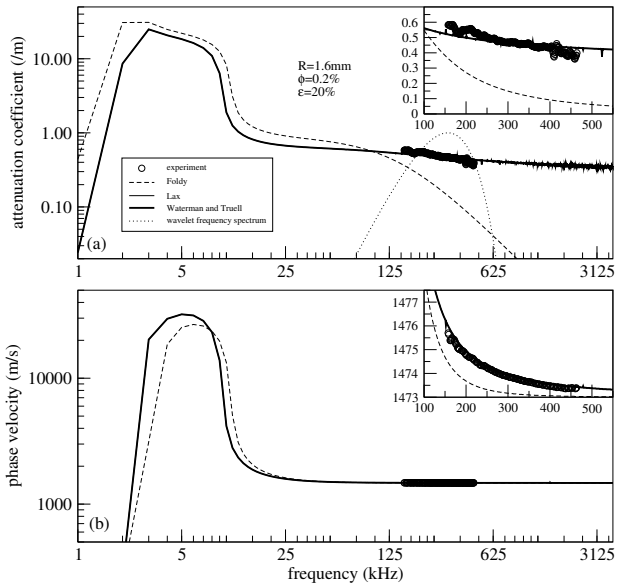

Figure 4: (a) Experimental attenuation coefficient and (b) phase velocity measured with a high frequency (peak frequency ν_0=310 kHz) acoustic pulse propagation across 740 mm of bubbly water (circles). Effective models by Foldy (dashed curve), Lax (thin curve) and Waterman and Truell (bold curve).

measurements (Fig. 4a, dashed curve): for frequencies as high as ν_{p_0}=310 kHz, air bubbles with r_0=1.6 mm can not be approximated to isotropic scatterers and the Foldy's model is not adapted for the present case study. The modeled attenuation based on k_L or k_{WT} are equivalent and in good agreement with the data (Fig. 4a, solid curves). In particular, the Lax's and Waterman and Truell's models correctly predict the weak decrease of α with the frequency. This means that bubbles act as anisotropic scatterers in the biphasic medium where multiple scattering can be neglected. The modeled phase velocities v based on k_L and k_{WT} are similar and in agreement with the data (Fig. 4b, solid curves).

4 Modeling based on a Gaussian derivative source wavelet

4.1 Fractional derivation and dilation factors based on $\alpha(\nu)$

The reference source signal $B_0(t)$ is similar to a Gaussian derivative wavelet with a derivative order β_0=4 [21]:

$$B_0(t) \sim S_0(t) \equiv \frac{d^{\beta_0}}{dt^{\beta_0}} e^{-\pi^2 \nu_0^2 (t-\tau_0)^2} \tag{10}$$

characterized by 5 extrema and symmetric relative to the maximum peak located at time τ_0, and a natural frequency

$$\nu_0 = \nu_{p_0}\sqrt{2/\beta_0} \tag{11}$$

where ν_{p_0}=310 kHz is the peak frequency. In the frequency domain, the wavelet can be expressed by

$$\hat{S}_0(\nu) = \left(\frac{\nu^2}{\nu_{p_0}^2} e^{1-\frac{\nu^2}{\nu_{p_0}^2}}\right)^{\frac{\beta_0}{2}} e^{i\left(-2\pi\nu\tau_0 + \pi\frac{\beta_0}{2}\right)} \tag{12}$$

and includes the normalization factor of the Gaussian derivative function [30], *i.e.* $|\hat{S}_0(\nu_{p_0})|$=1. Inside the bubbly water, the amplitude spectrum of the Fourier transform of the waveform $B_x(t)$

$$|\hat{B}_x(\nu)| = e^{-\alpha(\nu)x}\left(\frac{\nu^2}{\nu_{p_0}^2} e^{1-\frac{\nu^2}{\nu_{p_0}^2}}\right)^{\frac{\beta_0}{2}} \tag{13}$$

directly leads to $\alpha(\nu_{p_0}) = -\ln|\hat{B}_x(\nu_{p_0})|/x$, and the phase spectrum

$$\arg\left(\hat{B}_x(\nu)\right) = -2\pi\nu\left(\tau_0 + \frac{x}{v(\nu)}\right) + \frac{\pi}{2}\beta_0 \tag{14}$$

is characterized by a constant phase shift $\frac{\pi}{2}\beta_0$.

In the dominant frequency range of the experiment, an approximation of the phase velocity $v(\nu)$ is not obvious at this stage of the analysis but the attenuation coefficient can be approximated to

$$\alpha(\nu) \sim \tilde{\alpha}(\nu) = a - a'\ln\nu. \tag{15}$$

In this case, the amplitude spectrum can be approximated to

$$|\hat{B}_x(\nu)| \sim |\hat{\tilde{B}}_x(\nu)| = e^{-ax}\nu^{a'x}\left(\frac{\nu^2}{\nu_{p_0}^2} e^{1-\frac{\nu^2}{\nu_{p_0}^2}}\right)^{\frac{\beta_0}{2}} \tag{16}$$

which suggests that if $\frac{\partial a'}{\partial \nu} = 0$, the dispersive medium acts as a derivative filter with the order $a'x$. The parameters used in eq. 15 are a=1.44 m^{-1} and as a first approximation, $a'\ln\nu \simeq b\ln\nu_{p_0}$ with b=0.077 m^{-1}. In the close vicinity of ν_{p_0}, it can be shown analytically that

$$|\hat{\tilde{B}}_x(\nu)| = A_x\left(\frac{\nu^2}{\nu_{p_x}^2} e^{1-\frac{\nu^2}{\nu_{p_x}^2}}\right)^{\frac{\beta_0+bx}{2}} \tag{17}$$

with

$$A_x = e^{-x(a+\frac{b}{2})}\nu_{p_0}^{bx}\left(\frac{\beta_0+bx}{\beta_0}\right)^{\frac{\beta_0+bx}{2}}. \tag{18}$$

The amplitude spectrum of $B_x(t)$ is thus similar to the amplitude spectrum of a new Gaussian derivative function characterized by a derivative order $\beta_0 + bx$ and a peak frequency

$$\nu_{p_x} = \nu_{p_0}\sqrt{\frac{\beta_0+bx}{\beta_0}} = \nu_0\sqrt{\frac{\beta_0+bx}{2}}. \tag{19}$$

In one hand, the dispersion of the acoustic wave linearly increases the peak frequency from ν_{p_0}=310 kHz when x=0 to 312.5 kHz when x=740 mm, a very weak modification in agreement with the experimental results. In the other hand, the derivative order increases from β_0 when x=0 to 4.07 when x=740 mm, not in agreement with the lost of symmetry of the reference signal observed in the experiments (see Fig. 1). This means that the bubbly water can not be approximated to a simple derivative filter.

Actually, the natural frequency of the new Gaussian derivative wavelet may depend on x, *i.e.*

$$\nu_{p_x} = \nu_{0_x}\sqrt{\frac{\beta_x}{2}} \tag{20}$$

is associated to the derivative order

$$\beta_x = \frac{\nu_0^2}{\nu_{0_x}^2}\left(\beta_0 + bx\right) = \frac{\beta_0 + bx}{\delta_x^2} \tag{21}$$

where δ_x is a time-dilation factor. As a result, the peak frequency

$$\nu_{p_x} = \nu_{p_0}\delta_x\sqrt{\frac{\beta_x}{\beta_0}} \tag{22}$$

and the amplitude spectrum

$$|\hat{\tilde{B}}_x(\nu)| = A_x\left[\left(\frac{\nu^2}{\nu_{p_x}^2}e^{1-\frac{\nu^2}{\nu_{p_x}^2}}\right)^{\frac{\beta_x}{2}}\right]^{\delta_x^2} \tag{23}$$

depend on δ_x and β_x instead of the parameter b (eq. 21). Interestingly, by introducing here the derivative order

$$\gamma_x = \beta_x - \beta_0, \tag{24}$$

this can be generalized to

$$|\hat{\tilde{B}}_x(\nu)| = A'_x\left[\left|\hat{S}_0\left(\frac{\nu}{\delta_x}\right)\right|\left(\frac{\nu}{\delta_x}\right)^{\gamma_x}\right]^{\delta_x^2} \tag{25}$$

with

$$A'_x = e^{-ax-\frac{\beta_0}{2}\left(\delta_x^2-1\right)}\nu_{p_0}^{\beta_0\left(\delta_x^2-1\right)}\delta_x^{(\beta_0+\gamma_x)\delta_x^2}. \tag{26}$$

This puts in evidence that the dispersive medium induces both time derivation and dilation effects which compensate in the amplitude spectrum of the transmitted signal $B_x(t)$.

If $bx \ll \beta_0$, a condition satisfied in the present case study where $\tilde{\alpha}(\nu)$ is nearly a constant in the dominant frequency range of the source wavelet, the analytical approach gives

$$\delta_x^2\left(\beta_0 + \gamma_x\right) \simeq \beta_0 \tag{27}$$

and $\nu_{p_x} \simeq \nu_{p_0}$ in agreement with the experiments. The trivial solution $\gamma_x = 0$ and $\delta_x = 1$ is observed in the experiments only at x=0: to quantify δ_x and γ_x associated to waveform changes inside the dispersive medium, an analytical approximation of the phase velocity is required.

4.2 Corresponding analytical approximation of $v(\nu)$

The amplitude spectrum of the signal $B_x(t)$ measured inside the bubbly water is similar to $|\hat{\tilde{B}}_x(\nu)|$ characterized by both the fractional derivative order γ_x and the dilation factor δ_x applied to the Gaussian derivative source wavelet $S_0(t)$. As a first approach, the associated phase spectrum is written as

$$\arg\left(\hat{\tilde{B}}_x(\nu)\right) = \arg\left(\hat{S}_0\left(\frac{\nu}{\delta_x}\right)\right) + \frac{\pi}{2}\gamma_x - 2\pi\nu T'_x \tag{28}$$

where the travel time $T'_x = \frac{x}{v_0} + \tau'_x$ corresponds to the sum of the travel time in pure water and a supplementary time shift τ'_x to align the maximum amplitudes of $\tilde{B}_x(t)$ and $B_x(t)$. The approximation $\arg\left(\hat{B}_x(\nu)\right) \sim \arg\left(\hat{\tilde{B}}_x(\nu)\right)$ leads to the phase velocity approximation

$$v(\nu) \sim \tilde{v}(\nu) = v_0\left[1 + \frac{v_0}{x}\left(\tau_0\frac{1-\delta_x}{\delta_x} + \tau'_x - \frac{\gamma_x}{4\nu}\right)\right]^{-1}. \tag{29}$$

Actually, τ'_x depends on δ_x and γ_x and can be replaced by an equivalent time shift τ_x to write the phase spectrum as

$$\arg\left(\hat{\tilde{B}}_x(\nu)\right) = \arg\left(\hat{S}_0\left(\nu\right)\right) + \frac{\pi}{2}\gamma_x - 2\pi\nu\left(\frac{x}{v_0} + \tau_x\right) \tag{30}$$

and the phase velocity becomes

$$\tilde{v}(\nu) = v_0\left[1 + \frac{v_0}{x}\left(\tau_x - \frac{\gamma_x}{4\nu}\right)\right]^{-1}. \tag{31}$$

It is of first importance to highlight here that waveform changes measured inside the dispersive medium are related to the derivative order γ_x applied to the phase spectrum of the source signal. In these analytical approximations, the equivalent medium is characterized by an effective velocity defined by

$$\tilde{v}_0 = \lim_{\nu\to+\infty} \tilde{v}(\nu) \tag{32}$$

and a phase velocity $\tilde{v}(\nu)$ that should not depend on the propagation distance x, *i.e.* it is expected that $\gamma_x = \kappa_\gamma x$ and $\tau_x = \kappa_\tau x$ where the coefficients κ_γ and κ_τ are unknown.

Analytical developments to express γ_x and τ_x with respect to x are not straightforward. Instead, an optimization approach has been developed, based on a simulated annealing method to optimize the normalized correlation coefficient between $B_x(t)$ and $\tilde{B}_x(t)$ when the source signal is the theoretical wavelet $S_0(t)$ (peak frequency ν_{p_0}=310 kHz and derivative order β_0=4). The attenuation coefficient is approximated to $\tilde{\alpha}(\nu)$ and the phase velocity $v(\nu)$ is defined by the complex effective wavenumber $k_L(\nu)$. The numerical optimization, performed for propagation distances between 0 and 740 mm ($x \leq$0 stands for

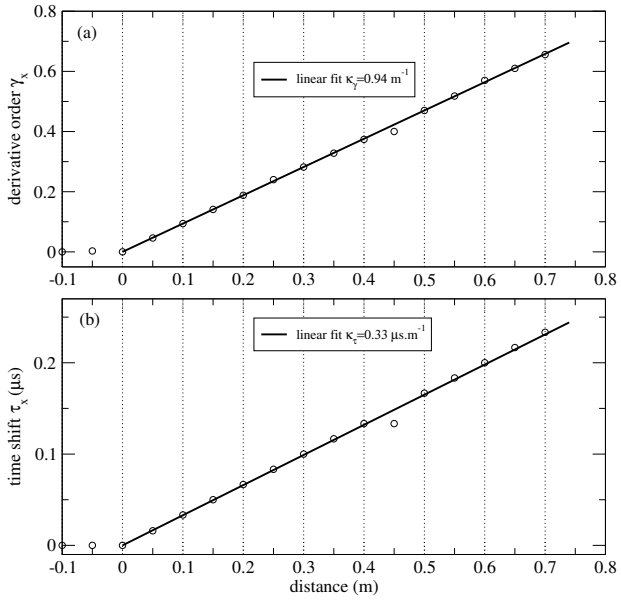

Figure 5: (a) Derivative order and (b) dilation factor of the optimized waveform $\tilde{B}_x(t)$ that best fits the acoustic waveform $B_x(t)$ measured at different distances inside the bubbly water (circles), and linear fits (solid lines).

propagation in water) highlights that κ_γ=0.94 m^{-1} and κ_τ=0.33 μs.m^{-1} (Figs.5a and b, respectively).

As a result, the effective and phase velocities actually do not depend on x and can be expressed as

$$\tilde{v}_0 = \frac{v_0}{1 + v_0 \kappa_\tau} \tag{33}$$

which is about $\tilde{v}_0 \simeq$1472.3 m.s^{-1} close to the sound speed in water, and

$$\tilde{v}(\nu) = \tilde{v}_0 \left[1 - \frac{\tilde{v}_0 \kappa_\gamma}{4\nu} \right]^{-1} \tag{34}$$

which is the analytical approximation of the phase velocity when the attenuation coefficient is approximated by $\tilde{\alpha}(\nu) = a - a' \ln \nu$.

4.3 Acoustic waveform modeling

The attenuation coefficient $\bar{\alpha}(\nu)$ (Fig. 6a1) and phase velocity $\bar{v}(\nu)$ (Fig. 6a2) that characterize the bubbly water effective properties are used to model the propagation of an acoustic source signal. The source signal is the theoretical wavelet $S_0(t)$ (Fig. 6b1). Changes of the waveforms with the propagation distance x (Fig. 6b2) are modeled by a simple phase shift $\frac{\pi}{2}\gamma_x$ that linearly increases with x with the factor κ_γ.

The waveform at x=740 mm illustrates the very good agreement with the waveform based on the complex wavenumber of the Lax's effective model (Fig. 7b3). Note that in

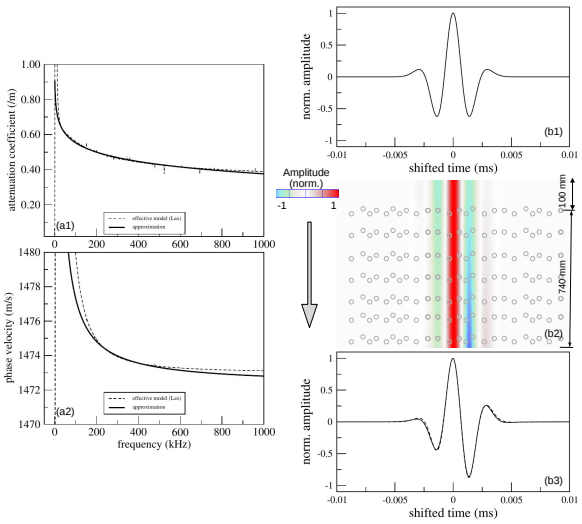

Figure 6: (a1-a2) Attenuation coefficient $\tilde{\alpha}(\nu)$ and phase velocity $\tilde{v}(\nu)$ (solid curves) used to approximate the effective model (dashed curves) based on Gaussian derivative function properties. (b1) Theoretical source wavelet $S_0(t)$ defined as a Gaussian derivative function with β_0=4. (b2) Modeling of the waveforms across the dispersive medium based on the derivative order γ_x (see Fig. 5a) applied to the phase of $S_0(t)$. (b3) Last waveform associated to $\gamma_x \simeq 0.7$ (solid curve) and waveform associated to the effective wavenumber (dashed curve).

this theoretical approach, the attenuation coefficient can be assessed by performing series of optimization procedures at x=740 mm (large distance to improve the result accuracy) without the limitation $bx \ll \beta_0$ and averaging the results based on eq. 21 to determine b: the parameter a can be assessed from the amplitude spectrum at the peak frequency.

5 Experimental high frequency acoustic waveforms across the bubbly water

The source signal is the experimental signal $B_0(t)$ (see Figs. 1b1 and 1b4). According to the previous theoretical developments, the amplitude spectrum of the transmitted signal $B_x(t)$ is similar to the one of the source signal as observed from the experimental measurements, and the phase spectrum is the one of the source signal plus a phase shift $\frac{\pi}{2}\gamma_x$. Note that γ_x may differ from the theoretical results because $B_0(t)$ is not a perfect Gaussian derivative function and the bubbly water is a dynamic dispersive medium which physical properties may be not homogeneous. The aim is characterizing the experimental waveform changes across the bubbly water by the use of γ_x defined from an optimization procedure.

As a first approximation, the result of the optimization is a linear increasing trend of the derivative order with x (Fig. 7a, circles): γ_x=1.1x in agreement with the theoretical developments based on a Gaussian derivative source wavelet (Fig. 7a, solid and dashed lines, respectively). This derivative order is applied to the signal $B_0(t)$ as a phase shift $\frac{\pi}{2}\gamma_x$ to model the waveforms across the bubbly water (Figs. 7b2), with a very good agreement with the measurements (see Fig. 1b2 and the particular case at x=740 mm displayed in Fig. 7b3).

Fluctuations of the experimental γ_x are related to the dynamic of the bubbly water that can also be observed from the waveform amplitude analyzed in the time domain (Section III.A, Fig. 3b, circles). Interestingly, both this attenuation and γ_x highlight a peak and a drop located at about x=10 mm and 550 mm, respectively: this suggests a correlation between these two attributes, with a nearly constant ratio about 0.2 (Fig. 8, circles). From the theoretical developments, the amplitude is quantified by the factor A_x and gives the linear fitted attenuation $-20\log_{10} A_x$=4x: the ratio between the derivative order γ_x and this attenuation is a constant about 0.23, in agreement with the experimental results (Fig. 8, dashed line).

6 Conclusion

The present work describes both acoustic experiments and analytical developments to quantify waveform changes of a pulse (peak frequency ν_{p_0}=310 kHz) that propagates (distance $x \leq$740 mm) inside a bubbly water composed of air bubbles (radius 1.6 mm, gas volume fraction 20%). This corresponds to high frequency acoustic experiments in a single scattering dispersive medium. In the time domain, the decrease of the waveform amplitude with x is quantified by attenuation properties and qualitatively associated to changes of

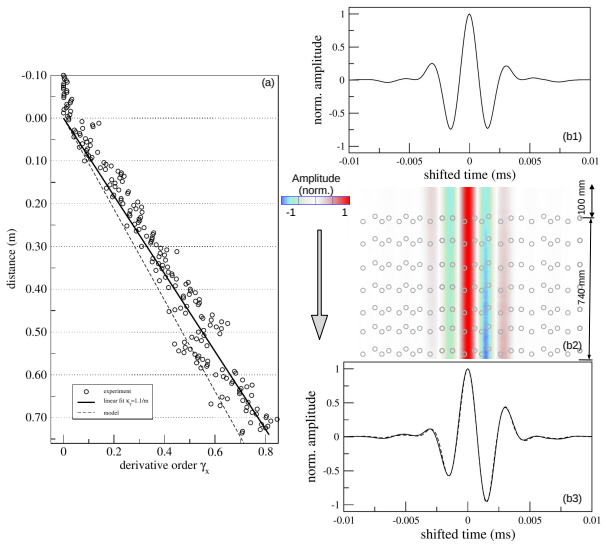

Figure 7: (a) Experimental derivative order γ_x across the bubbly water (circles): linear fits for the dynamic and theoretical static dispersive media (solid and dashed lines, respectively). (b1) Experimental source signal $B_0(t)$. (b2) Modeling of the waveforms across the dispersive medium based on the derivative order γ_x (a) applied to the phase of $B_0(t)$. (b3) Last waveform associated to $\gamma_x \simeq 0.7$ (solid curve) and waveform associated to the effective wavenumber (dashed curve).

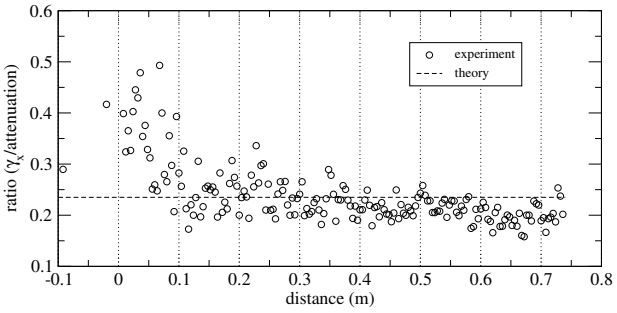

Figure 8: Experimental ratio (circles) between the derivative order γ_x and the attenuation of the waveform amplitude (Fig. 3b) as a function of the propagation distance inside the bubbly water, and theoretical ratio (dashed line) based on a Gaussian derivative source wavelet.

the waveform shape. In the frequency domain, the amplitude spectrum is nearly constant and does not depend on x. Effective medium theories are used to define the attenuation coefficient $\alpha(\nu)$ and phase velocity $\alpha(\nu)$ in agreement with the experimental results. In the high frequency range defined by the acoustic pulse, $\alpha(\nu)$ is nearly constant. In the framework of Gaussian derivative functions with a source wavelet characterized by a derivative order β_0=4, it is demonstrated that $\tilde{\alpha}(\nu)$ acts as a fractional derivative order $0 \leq \gamma_x \leq 0.8$ and a dilation factor $\delta_x \simeq \sqrt{\beta_0/(\beta_0+\gamma_x)}$. A numerical optimization method highlights that $\gamma_x = \kappa_\gamma x$, with κ_γ=0.94 m^{-1}. The approximation of the associated phase velocity can be written as $\tilde{v}(\nu) = \tilde{v}_0/(1-\tilde{v}_0\kappa_\gamma/4\nu)$ where $\tilde{v}_0$ is close to the sound speed in water. Based on the experimental measurements, it is also shown that the waveform shape quantified by the derivative order γ_x is proportional to the waveform amplitude which decreases with the propagation distance x across the dispersive medium.

The effects induced by the time derivation (γ_x) and time dilation (δ_x) compensate in the amplitude spectrum but the former dominates in the phase spectrum according to the phase shift $\frac{\pi}{2}\gamma_x$. This highlights a particular property of dispersive media characterized by $\tilde{\alpha}$ (eq. 15) and $\tilde{v}$ (eq. 34): if $bx \ll \beta_0$, the acoustic waveform associated to the propagation distance x is similar to the source signal when $\pi\gamma_x = \pi\kappa_g x = 4\pi n$, where n is an integer. For the present case study, this means that the shapes of the acoustic waveforms recorded as a function of the propagation distance inside the bubbly water differ by a linear increasing phase shift and are similar every 4.25 meters. This theoretical acoustic phenomenon may be of first interest in underwater communication, including the few kHz-acoustic pulses emitted by echosounders or marine mammals across mm-radius bubbles in the surrounding of active gas seeps for instance.

References

[1] Michael A Ainslie and Timothy G Leighton. "Review of scattering and extinction cross-sections, damping factors, and resonance frequencies of a spherical gas bubble". In: *J. Acoust. Soc. Am.* 130.5 (2011), pp. 3184–3208.

[2] Habib Ammari, Brian Fitzpatrick, David Gontier, Hyundae Lee, and Hai Zhang. "Minnaert resonances for acoustic waves in bubbly media". In: *Annales de l'Institut Henri Poincaré C, Analyse non linéaire*. Vol. 35. 7. Elsevier. 2018, pp. 1975–1998.

[3] Victor C Anderson. "Sound scattering from a fluid sphere". In: *J. Acoust. Soc. Am.* 22.4 (1950), pp. 426–431.

[4] Keita Ando, Tim Colonius, and Christopher E Brennen. "Improvement of acoustic theory of ultrasonic waves in dilute bubbly liquids". In: *J. Acoust. Soc. Am.* 126.3 (2009), EL69–EL74.

[5] Clarence Samuel Clay and Herman Medwin. "Acoustical oceanography: principles and applications". In: (1977).

[6] Kerry W Commander and Andrea Prosperetti. "Linear pressure waves in bubbly liquids: Comparison between theory and experiments". In: *J. Acoust. Soc. Am.* 85.2 (1989), pp. 732–746.

[7] Martin Devaud, Thierry Hocquet, Jean-Claude Bacri, and Valentin Leroy. "The Minnaert bubble: an acoustic approach". In: *European Journal of Physics* 29.6 (2008), p. 1263.

[8] Jean-Baptiste Doc, Jean-Marc Conoir, Régis Marchiano, and Daniel Fuster. "Nonlinear acoustic propagation in bubbly liquids: Multiple scattering, softening and hardening phenomena". In: *J. Acoust. Soc. Am.* 139.4 (2016), pp. 1703–1712.

[9] Ramani Duraiswami, Sankar Prabhukumar, and Georges L Chahine. "Bubble counting using an inverse acoustic scattering method". In: *J. Acoust. Soc. Am.* 104.5 (1998), pp. 2699–2717.

[10] Vincent Duro, Dominique Raphaël Rajaona, Dominique Décultot, and Gérard Maze. "Experimental study of sound propagation through bubbly water: comparison with optical measurements". In: *IEEE Journal of Oceanic Engineering* 36.1 (2011), pp. 114–125.

[11] Yuzhe Fan, Haisen Li, Chao Xu, and Tian Zhou. "Influence of bubble distributions on the propagation of linear waves in polydisperse bubbly liquids". In: *J. Acoust. Soc. Am.* 145.1 (2019), pp. 16–25.

[12] L.L. Foldy. "The multiple scattering of waves". In: *Phys. Rev.* 67 (1945), pp. 107–119.

[13] Francis E Fox, Stanley R Curley, and Glenn S Larson. "Phase velocity and absorption measurements in water containing air bubbles". In: *J. Acoust. Soc. Am.* 27.3 (1955), pp. 534–539.

[14] Peter JA Frinking, Nico de Jong, and E Ignacio Cespedes. "Scattering properties of encapsulated gas bubbles at high ultrasound pressures". In: *J. Acoust. Soc. Am.* 105.3 (1999), pp. 1989–1996.

[15] Daniel Fuster, Jean-Marc Conoir, and T Colonius. "Effect of direct bubble-bubble interactions on linear-wave propagation in bubbly liquids". In: *Phys. Rev. E* 90.6 (2014), p. 063010.

[16] Walter I Futterman. "Dispersive body waves". In: *J. Geophys. Res.* 67.13 (1962), pp. 5279–5291.

[17] DE Goertz, ME Frijlink, MM Voormolen, Nico de Jong, and AFW van der Steen. "High frequency attenuation measurements of lipid encapsulated contrast agents". In: *Ultrasonics* 44 (2006), e131–e134.

[18] Lars Hoff, Per C Sontum, and Jens M Hovem. "Oscillations of polymeric microbubbles: Effect of the encapsulating shell". In: *J. Acoust. Soc. Am.* 107.4 (2000), pp. 2272–2280.

[19] S. Ker and Y. Le Gonidec. “Fractional integration of seismic wavelets in anelastic media to recover multiscale properties of impedance discontinuities”. In: *Geophysics* 83 (2018), pp. 61–71.

[20] M. Lax. “Multiple scattering of waves”. In: *Rev. Mod. Phys.* 23 (1951), pp. 287–310.

[21] Y. Le Gonidec, D. Gibert, and J.-N. Proust. “Multiscale Analysis of waves reflected by complex interfaces : basic principles and experiments”. In: *J. Geophys. Res.* 107.doi:10.1029/2006JB004518 (2002).

[22] V. Leroy, A. Strybulevych, and J.H. Page. “Sound velocity and attenuation in bubbly gels measured by transmission experiments”. In: *J. Acoust. Soc. Am.* ().

[23] Bin Liang, Xinye Zou, and Jianchun Cheng. “Effective medium method for sound propagation in a soft medium containing air bubbles”. In: *J. Acoust. Soc. Am.* 124.3 (2008), pp. 1419–1429.

[24] Alexandra M Padilla and Thomas C Weber. “Acoustic backscattering observations from non-spherical gas bubbles with ka between 0.03 and 4.4”. In: *J. Acoust. Soc. Am.* 149.4 (2021), pp. 2504–2519.

[25] Andrea Prosperetti. “Thermal effects and damping mechanisms in the forced radial oscillations of gas bubbles in liquids”. In: *J. Acoust. Soc. Am.* 61.1 (1977), pp. 17–27.

[26] Jacob Rubinstein. “Bubble interaction effects on waves in bubbly liquids”. In: *J. Acoust. Soc. Am.* 77.6 (1985), pp. 2061–2066.

[27] Edward Silberman. “Sound velocity and attenuation in bubbly mixtures measured in standing wave tubes”. In: *J. Acoust. Soc. Am.* ().

[28] HR Suiter. “Pulse length effects on the transmissivity of bubbly water”. In: *J. Acoust. Soc. Am.* 91.3 (1992), pp. 1383–1387.

[29] Tony Valier-Brasier, Jean-Marc Conoir, Francois Coulouvrat, and Jean-Louis Thomas. “Sound propagation in dilute suspensions of spheres: Analytical comparison between coupled phase model and multiple scattering theory”. In: *J. Acoust. Soc. Am.* 138.4 (2015), pp. 2598–2612.

[30] Y. Wang. “Generalized seismic wavelets”. In: *Geophys. J. Int.* 203 (2015), pp. 1172–1178.

[31] P.C. Waterman and R. Truell. “Multiple scattering of waves”. In: *J. Math. Physics* 2 (1961), pp. 512–537.

[32] Preston S Wilson, Ronald A Roy, and William M Carey. “Phase speed and attenuation in bubbly liquids inferred from impedance measurements near the individual bubble resonance frequency”. In: *J. Acoust. Soc. Am.* 117.4 (2005), pp. 1895–1910.

[33] Z. Ye. “Acoustic dispersion and attenuation in many spherical scatterer systems and the kramers-Kronig relations”. In: *J. Acoust. Soc. Am.* 101 (1997), pp. 3299–3305.